An orthogonal c-Cbl recognition mode targets LynA for rapid degradation and builds specificity into the LynA checkpoint

Ben F. Brian IV[1], Myra G. Nunez[1], Kathryn L. Schwertfeger[1,2,3], Tanya S. Freedman[1,2,4,*]

[1]Department of Pharmacology, University of Minnesota, Minneapolis, MN 55455, USA.

[2]Center for Immunology and Masonic Cancer Center, University of Minnesota, Minneapolis, MN 55455, USA.

[3]Department of Laboratory Medicine and Pathology, University of Minnesota, Minneapolis, MN 55455, USA.

[4]Center for Autoimmune Diseases Research, University of Minnesota, Minneapolis, MN 55455, USA.

[*]To whom correspondence should be addressed: tfreedma@umn.edu

Abstract

The activity of Src-family kinases (SFKs), which phosphorylate immunoreceptor tyrosine-based activation motifs (ITAMs), is critical factor regulating myeloid-cell activation. In a previous paper (Freedman *et al.*, 2015) we showed in macrophages that the SFK LynA is uniquely susceptible to rapid ubiquitin-mediated degradation, functioning as a rheostat regulating ITAM signaling. We now report the mechanism by which LynA is preferentially targeted for degradation and how cell specificity is built into the LynA rheostat. Using genetic and biochemical analysis, we found that the E3 ubiquitin ligase c-Cbl preferentially targets LynA via tyrosine 32 in its unique insert region. This orthogonal mode of c-Cbl recognition depresses the steady-state level of macrophage LynA. Mast cells, however, express little c-Cbl and have correspondingly high steady-state levels of LynA. Upon activation, mast-cell LynA is not rapidly degraded, and SFK-mediated signaling is amplified relative to macrophages. Cell-specific c-Cbl expression therefore builds cell specificity into the LynA checkpoint.

Introduction

Phosphorylation of immunoreceptor tyrosine-based activation motifs (ITAMs) by Src-family kinases (SFKs) is the first step in the activation of an innate immune response during a pathogen encounter. Initiation of cell-activating signaling typically occurs within clusters of ITAM-coupled receptors such as

26 FcγR (1) or the hemi-ITAM Dectin-1 (2, 3), nucleated by highly multivalent binding to immunoglobulin-
27 G-decorated pathogens or fungal cell-wall β-glucans respectively. Together, SFKs and phosphorylated
28 ITAMs trigger activation of the tyrosine kinase Syk (4). The SFKs and Syk then drive activation of
29 membrane-proximal signaling through adaptor proteins, cytoskeleton-modulating proteins such as the
30 FAK/Pyk2 kinases and Paxillin, and Tec kinases, which activate second-messenger pathways via
31 phosphoinositide 3-kinase and phosphoinositide phospholipases Cγ (PI3K and PLCγ1/2 respectively).
32 Ultimately, these early events lead to downstream signaling through Erk1/2 and other pathways (4). As
33 the byproducts of activated macrophages can be toxic (*e.g.* release of reactive oxygen species) and
34 drive inflammation (*e.g.* release of tumor necrosis factor α), the responsiveness of innate immune cells
35 must be tightly regulated (5-8).

36 Multiple mechanisms work together to tune the responsiveness of macrophages and other myeloid
37 cells, including negative regulation by the phosphatases CD45 and CD148 (5, 9, 10), cytoskeletal
38 barriers to diffusion (11), signaling via immunoreceptor tyrosine inhibitory motifs (ITIMs) (12) and
39 inhibitory ITAMs (13, 14), and degradation and mislocalization of signaling molecules targeted for
40 polyubiquitination by ubiquitin ligases (15, 16). The SFKs, which in myeloid cells typically include Fgr,
41 Fyn, and two splice forms each of Hck and Lyn, may also have positive and negative functions (12, 17-
42 19). Layered onto the traditional positive- and negative-regulatory roles of the SFKs, we have shown
43 that activated LynA (the longer of the two Lyn splice forms) is rapidly and specifically targeted for
44 polyubiquitination and degradation, forming the basis of a signaling checkpoint that blocks spurious
45 macrophage activation (20). The mechanism preferentially targeting LynA for polyubiquitination and the
46 molecular basis of this selectivity have not been elucidated previously.

47 Unlike Dectin-1 and FcγR signaling in macrophages, which is typically triggered in the context of
48 pathogen-induced μm-scale clusters of receptors (5, 9, 20), mast-cell FcεR signaling has a low
49 threshold for activation-- small or even monovalent antigen-IgE complexes are sufficient to induce a
50 signaling response (21, 22). Like macrophages, mast cells express LynA, and this disparity in receptor
51 sensitivity has not previously been explained.

52 This paper describes the mechanism by which active LynA is selectively recognized and rapidly
53 degraded, tuning its activation kinetics and its steady-state protein levels in a cell-specific manner. To
54 reveal the requirements for LynA degradation, we synchronized receptor-independent SFK activation
55 using the designer inhibitor 3-IB-PP1 (23-25), which specifically inhibits a variant of the SFK-inhibitory
56 kinase Csk (Csk^{AS}) (20, 25, 26). Csk is responsible for phosphorylating a key inhibitory tyrosine in the
57 C-terminus of all the SFKs. Inhibiting Csk^{AS} leads to rapid and robust SFK activation due to the loss of
58 the dynamic equilibrium between Csk and the phosphatases CD45 and CD148 (27, 28). We showed
59 previously that SFK activation induced via 3-IB-PP1 treatment leads to the phosphorylation of the E3
60 ubiquitin ligase c-Cbl and the preferential polyubiquitination and degradation of the SFK LynA, but it
61 was not clear whether these two events were linked. Using knockdown, overexpression, and genetic
62 models, we now demonstrate that c-Cbl, but not its homolog Cbl-b, controls the steady-state expression
63 of LynA and mediates its rapid degradation upon activation in macrophages. LynA is targeted by c-Cbl
64 via a phosphorylation site, Tyr32 within its unique region, a mode of interaction distinct from the slower-
65 phase action of c-Cbl and other E3 ligases on LynB and the other SFKs. Finally, we have discovered
66 that the LynA checkpoint is cell specific. In mast cells, which express very little c-Cbl but abundant Cbl-
67 b, LynA is not rapidly degraded upon activation, helping to explain why mast cells have a lower
68 activation threshold than macrophages.

69 Results

70 c-Cbl mediates steady-state and activation-induced degradation of LynA in macrophages

71 We reported previously that activated LynA is rapidly polyubiquitinated and degraded in Csk^{AS}
72 macrophages treated with the Csk^{AS} inhibitor (SFK activator) 3-IB-PP1 (20). To identify the responsible
73 E3 ubiquitin ligase, we tested the effects of knocking down the expression of candidate ligases using
74 small interfering (si)RNA. Csk^{AS} bone-marrow-derived macrophages (BMDMs) were transfected with
75 non-targeting control RNA or with siRNA constructs targeting c-Cbl or Cbl-b, known modulators of ITAM
76 signaling in both adaptive and innate immune cells (12, 15, 29). Resting Csk^{AS} BMDMs were treated

77 with 3-IB-PP1 for up to 5 min to activate the SFKs and initiate bulk degradation of LynA. Immunoblots
78 of whole-cell lysates showed efficient and specific knockdown **(Figure 1A)** of c-Cbl protein (70%
79 reduced) and Cbl-b protein (60% reduced) **(Figure 1B)**.

80 Knockdown of c-Cbl led to a delay in the degradation of activated LynA, with 1 min 3-IB-PP1 treatment
81 reducing LynA by 30% in c-Cbl knockdown BMDMs compared to 61% and 64% in Cbl-b knockdown
82 and control BMDMs, respectively **(Figure 1C)**. c-Cbl knockdown also increased the level of steady-
83 state LynA by 60% **(Figure 1D)**. The impaired degradation and increased steady-state LynA expression
84 together resulted in pronounced elevations in LynA protein in the first minutes of 3-IB-PP1 treatment;
85 after 1 min of 3-IB-PP1 treatment, LynA was elevated 2.9-fold in cCbl-deficient BMDMs relative to
86 control. Although it has been shown previously that c-Cbl and Cbl-b can have redundant functions (30,
87 31), we were unable to detect any role for Cbl-b in the steady-state or activation-induced degradation of
88 LynA.

89 To test whether the residual LynA degradation was due to incomplete knockdown, we also generated
90 *Csk^{AS}Cbl$^{-/-}$* mice to test LynA degradation in BMDMs lacking any c-Cbl expression. As with siRNA
91 knockdown, total c-Cbl knockout impaired LynA degradation in BMDMs **(Figure 1E)**; Cbl-b expression
92 in Csk^{AS}c-Cbl$^{-/-}$ BMDMs remained comparable to wild-type levels **(Figure 1F)**. Complete loss of c-Cbl
93 caused a more profound impairment of LynA degradation during the first few minutes of 3-IB-PP1
94 treatment **(Figure 1G)** a dramatic increase in steady-state LynA protein (up to 6-fold higher than in c-
95 Cbl$^{+/+}$ cells, **Figure 1H**). As in the knockdown experiments, LynA degradation in c-Cbl$^{-/-}$ BMDMs was not
96 fully eliminated but occurred on a much slower timescale, similar to the degradation of the other SFKs
97 (20). From this observation we conclude that c-Cbl is solely responsible for the rapid-phase degradation
98 unique to LynA, whereas other E3 ubiquitin ligases can complement c-Cbl to mediate slower-phase
99 SFK degradation. Although activating Syk phosphorylation was increased in Csk^{AS}c-Cbl$^{-/-}$ BMDMs
100 relative to Csk^{AS} BMDMs treated with 3-IB-PP1 **(Figure 1E)**, Erk phosphorylation after SFK activation
101 was paradoxically impaired **(Figure 1–figure supplement 1)**, likely due to the loss of the adaptor
102 function of c-Cbl in PI3K signaling (32, 33).

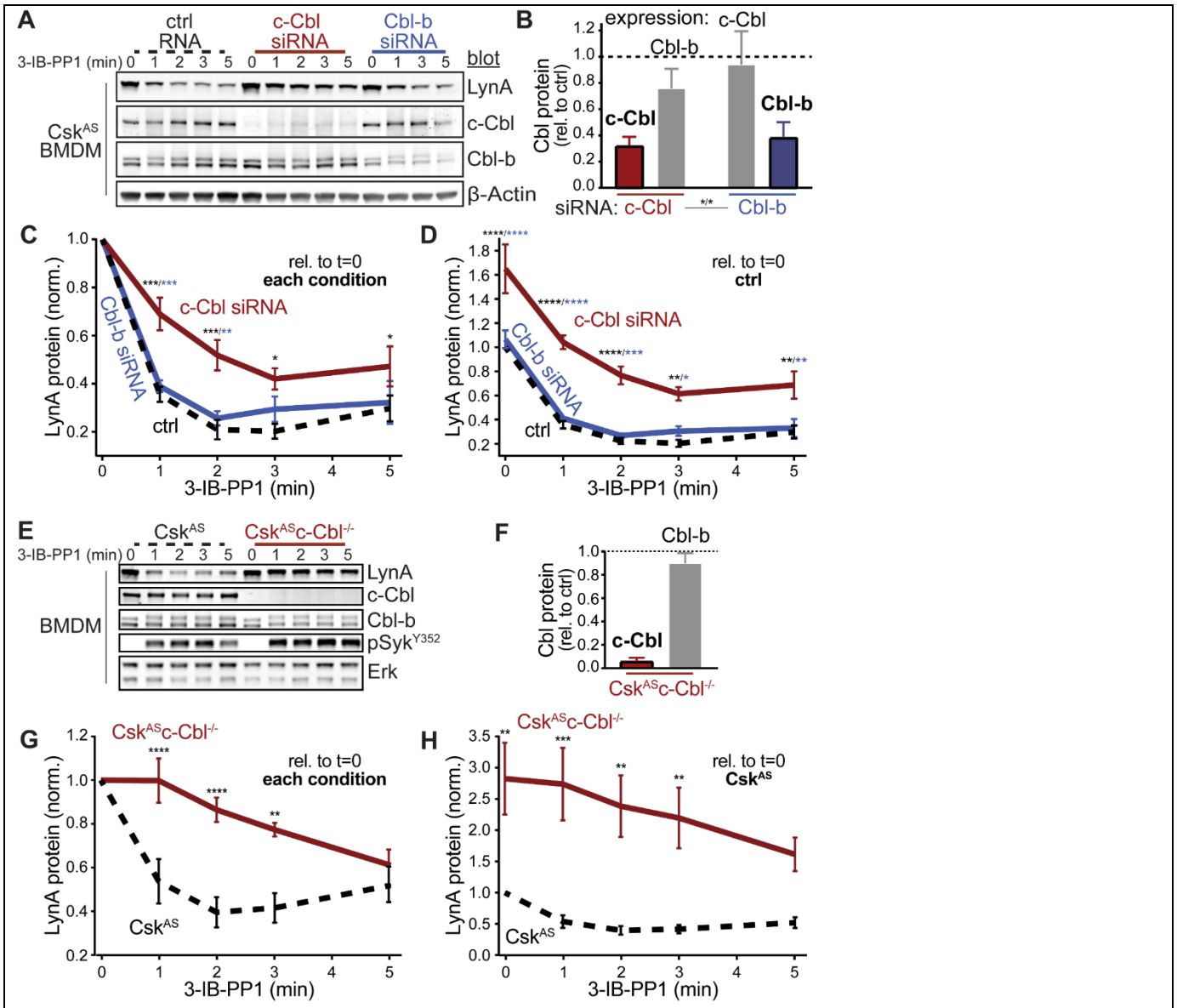

Figure 1. **Loss of c-Cbl expression in macrophages leads to steady-state upregulation and delayed degradation of LynA protein. (A)** Immunoblots showing LynA and Cbl protein content of Csk^{AS} BMDMs transfected with non-targeting control RNA (ctrl, black) or siRNA sequences targeting c-Cbl (red) or Cbl-b (blue). After overnight incubation, cells were treated with 3-IB-PP1 for the indicated times; β-actin is shown as a loading control. **(B-D)** Densitometry quantification of relative Cbl and LynA protein levels, corrected for total protein content. Error bars reflect standard error of the mean (SEM), n=3. **(B)** Quantification of c-Cbl and Cbl-b relative to ctrl expression of each (dotted line). Significant differences (Sig.) from two-way ANOVA with Sidak's multiple comparison test (asterisks): [c-Cbl expression: c-Cbl vs. Cbl-b siRNA samples], [Cbl-b expression: c-Cbl vs. Cbl-b siRNA samples]; *

113 P=0.0217-0.0473. **(C-D)** Quantification of LynA relative to t=0 within each siRNA condition **(C)** or the
114 steady-state level in the ctrl **(D)**. Sig. from two-way ANOVA with Tukey's multiple comparison test: [c-
115 Cbl vs. ctrl, black asterisks], [c-Cbl vs. Cbl-b, blue asterisks]; **** P<0.0001, *** P=0.0001-0.0005, **
116 P=0.0015-0.0058, * P=0.0105-0.0451. No significant differences (ns) between other pairs. **(E)**
117 Immunoblots showing LynA and Cbl protein content of Csk^{AS} and Csk^{AS}c-$Cbl^{-/-}$ BMDMs treated with 3-
118 IB-PP1; Erk1/2 is shown as a loading control. **(F-H)** Quantification of relative Cbl and LynA protein
119 levels, corrected for total protein content. SEM, n=5. **(F)** Quantification of c-Cbl and Cbl-b in Csk^{AS}c-Cbl^{-}
120 $^{/-}$ BMDMs relative to expression levels in Csk^{AS} BMDMs (dotted line). **(G-H)** Quantification of LynA
121 relative to t=0 for each genotype **(G)** or the steady-state level in Csk^{AS} BMDMs **(H)**. Sig. from two-way
122 ANOVA with Tukey's multiple comparison test: [Csk^{AS} vs. Csk^{AS}c-$Cbl^{-/-}$, asterisks]; **** P<0.0001, ***
123 P=0.0004, ** P=0.0014-0.0048. Paradoxical loss of Erk signaling in c-Cbl-deficient cells is shown in
124 Figure 1–figure supplement 1. Refer to Figure 1–Source Data 1.

125 **A tyrosine residue in the unique-region insert of LynA is required for its rapid degradation**

126 Susceptibility to rapid, activation-induced degradation differentiates LynA from the splice variant LynB
127 and the other macrophage SFKs. Hck, Fgr, LynB, and Fyn (17, 19), are degraded >10-fold more slowly
128 than LynA during 3-IB-PP1 treatment (20) **(Figure 2A)**. Although not expressed in macrophages, Lck is
129 also degraded more slowly than LynA **(Figure 2B)**.

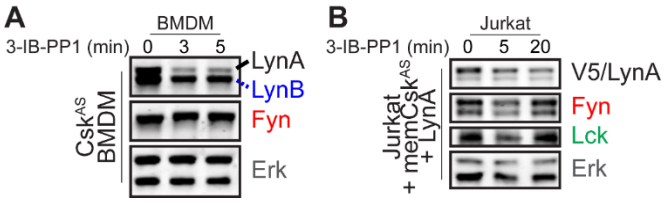

130

131 **Figure 2. Fyn and Lck are not rapidly degraded upon activation.** Immunoblots and quantification of
132 protein levels of Fyn, Lck, and LynB in 3-IB-PP1-treated Csk^{AS} BMDMs **(A)** and Jurkat cells **(B)**. Total
133 Erk1/2 protein (Erk) is a loading control.

134 As we have been unable to overexpress LynA in BMDMs by transfection, by Amaxa nucleofection, or
135 by lentiviral transduction, we expressed LynA ectopically in Jurkat T cells by transient transfection along
136 with a Cbl construct and a membrane-localized construct of Csk^{AS} ($memCsk^{AS}$) (25), which sensitizes
137 Jurkat cells to 3-IB-PP1 for synchronized SFK activation. As a proof of principle for this model system,
138 we transfected Jurkat cells with wild-type LynA, $memCsk^{AS}$, and empty vector (ctrl), c-Cbl, or Cbl-b
139 plasmid DNA **(Figure 3A)**, which increased c-Cbl expression 3-fold and Cbl-b 25-fold relative to
140 endogenous levels **(Figure 3B)**. Overexpressing one Cbl family member did not affect the abundance
141 of the other. As predicted, c-Cbl overexpression in Jurkat cells increased the rate of LynA degradation
142 (30% depleted after 5 min 3-IB-PP1 treatment in c-Cbl-overexpressing Jurkat cells vs. 10% and 0% in
143 ctrl and Cbl-b-overexpressing cells, respectively) **(Figure 3C)**. This observation is consistent with our
144 siRNA experiments in BMDMs, suggesting that Jurkat cells, which do not normally express Lyn, are
145 capable of supporting rapid, c-Cbl-mediated degradation of LynA.

146 LynB, which lacks a 21 amino-acid insert found in the unique region of LynA **(Figure 3D)**, was less
147 efficiently degraded in c-Cbl-transfected Jurkat cells **(Figure 3E)**, depleted by 10% (LynB) vs. 40%
148 (LynA) from baseline after 5 min 3-IB-PP1 **(Figure 3F)**. These data mirror our findings in Csk^{AS} BMDMs
149 (20) and confirm that the unique sensitivity of LynA to rapid degradation is preserved in the Jurkat
150 model. We hypothesized that the targeting site in LynA must lie within the unique-region insert
151 (residues 23-43) lacking in LynB (34, 35), which contains a tyrosine phosphorylation site (Tyr32) (36), a
152 predicted ubiquitination site (Lys40) (UbPred, 37), and a predicted threonine phosphorylation site
153 (Thr27) (NetPhos 3.1, 38) **(Figure 3D)**.

154 Substituting LynA Tyr32 with either alanine or phenylalanine completely blocked its rapid degradation
155 **(Figure 3E)**, reducing the depletion after 5 min 3-IB-PP1 from 40% (wt) to 10% ($LynA^{Y32A}$) or 8%
156 ($LynA^{Y32F}$) from baseline, levels indistinguishable from LynB **(Figure 3F)**. In contrast, mutation of the
157 predicted ubiquitination ($LynA^{K40R}$) or threonine phosphorylation ($LynA^{T27A}$) sites **(Figure 3E)** did not
158 impair LynA degradation **(Figure 3F)**.

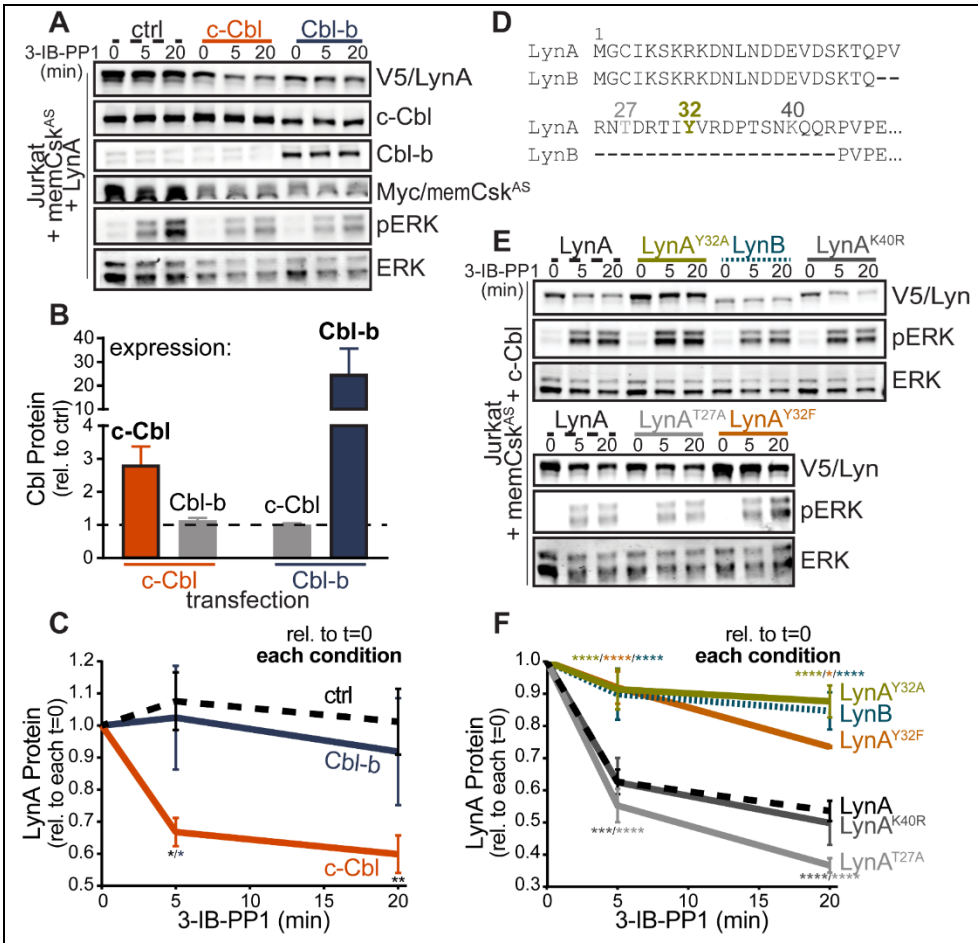

Figure 3. A unique tyrosine residue is required for activation-induced degradation of LynA. (A) Immunoblots of Jurkat cells cotransfected with V5-tagged LynA, Myc-tagged memCsk^{AS}, and either empty vector (ctrl, black dotted), c-Cbl (orange), or Cbl-b (blue) and treated with 3-IB-PP1. Activating phosphorylation (Thr202/Tyr204) of ERK1/2 (pERK) shows activating signaling, and total ERK1/2 (ERK) shows lane loading. **(B-C)** Quantification of relative Cbl and LynA protein, corrected for total protein content. SEM, n=4. **(B)** Quantification of overexpressed c-Cbl and Cbl-b relative to endogenous (ctrl) levels (dotted line). **(C)** Quantification of LynA protein during 3-IB-PP1 treatment relative to the steady-state level. Sig. from two-way ANOVA with Tukey's multiple comparison test: [c-Cbl vs. ctrl, black asterisks], [c-Cbl vs. Cbl-b, blue asterisks]; ** P=0.0092, * P=0.0270-0.0102. Other pairs ns. **(D)** N-terminal amino-acid sequences of mouse LynA and LynB (34, 35), including the 21 amino-acid unique insert of LynA. Tyrosine 32 (olive), threonine 27 (light gray), and lysine 40 (dark gray) are labeled. **(E)** Immunoblots of 3-IB-PP1-treated Jurkat cells cotransfected with c-Cbl, Myc-tagged memCsk^{AS}, and V5-tagged Lyn constructs, including wild-type LynA (black, dashed), LynA^{Y32A} (olive),

173 LynB (teal, dotted), LynA^{K40R} (dark gray), LynA^{T27A} (light gray), or LynA^{Y32F} (orange). **(F)** Quantification
174 of LynA protein levels, corrected for total protein, relative to the steady-state level. SEM, n=7 for LynA,
175 n=4 for LynA^{Y32A} and LynB; n=3 for LynA^{K40R}, LynA^{T27A}, and LynA^{Y32F}. Sig. from two-way ANOVA with
176 Tukey's multiple comparison test: [LynA^{Y32A} vs. LynA, olive asterisks], [LynB vs. LynA, teal asterisks],
177 [LynA^{Y32F} vs. LynA, orange asterisks], [LynA^{K40R} vs. LynA^{Y32A}, dark gray asterisks], [LynA^{T27S} vs.
178 LynA^{Y32A}, light gray asterisks]; **** P<0.0001, *** P=0.0006, * P=0.0166. ns: [LynA^{T27S} and LynA^{K40R} vs.
179 each other and LynA] and [LynA^{Y32A} and LynA^{Y32F} vs. each other and LynB]. Note: the error bar for
180 LynA^{Y32F} is smaller than the line width. Relative expression levels of LynA variants and LynB are shown
181 in Figure 3–figure supplement 1. Refer to Figure 3–Source Data 1.

182 As in BMDMs, the efficiency of Lyn degradation also affects its steady-state expression in Jurkat cells.
183 LynB is 2- and LynA^{Y32A} 3-fold more highly expressed than wild-type LynA, LynA^{K40R}, or LynA^{T27A} in
184 resting cells, resulting in 3- to 4-fold more protein remaining after 20 min treatment with 3-IB-PP1
185 **(Figure 3–figure supplement 1)**. Overall, we conclude that the unique tyrosine residue in the LynA
186 insert, a known site of tyrosine phosphorylation (36), is the recognition site for rapid, c-Cbl-mediated
187 degradation, and that this mechanism determines the half-life of activated LynA protein within an ITAM
188 signaling complex and tunes the steady-state expression of LynA protein. This suggests that c-Cbl-
189 mediated regulation of steady-state LynA protein levels occurs as a direct effect of c-Cbl protein activity
190 rather than merely a transcriptional feedback effect.

191 **LynA kinase activity is required for its rapid degradation**

192 SFK activation is a requirement for rapid degradation of LynA protein in BMDMs (20), but whether this
193 is direct effect of the LynA kinase itself or initiated by feedback from downstream signaling proteins has
194 been unclear. To investigate the role of LynA kinase activity in its degradation, we tested two
195 functionally impaired LynA constructs. First, we introduced a lysine residue in place of an activation-
196 loop threonine (T410K, c-Src residue 429 (39)) to disrupt substrate recognition (40). Second, we
197 introduced a phenylalanine residue in place of the activation-loop tyrosine, a known site of interaction

198 between the phosphotyrosine binding (PTB) domain of c-Cbl and Src (41) and the key

199 autophosphorylation site that stabilizes the active state (27, 42) (Y397F, c-Src residue 416).

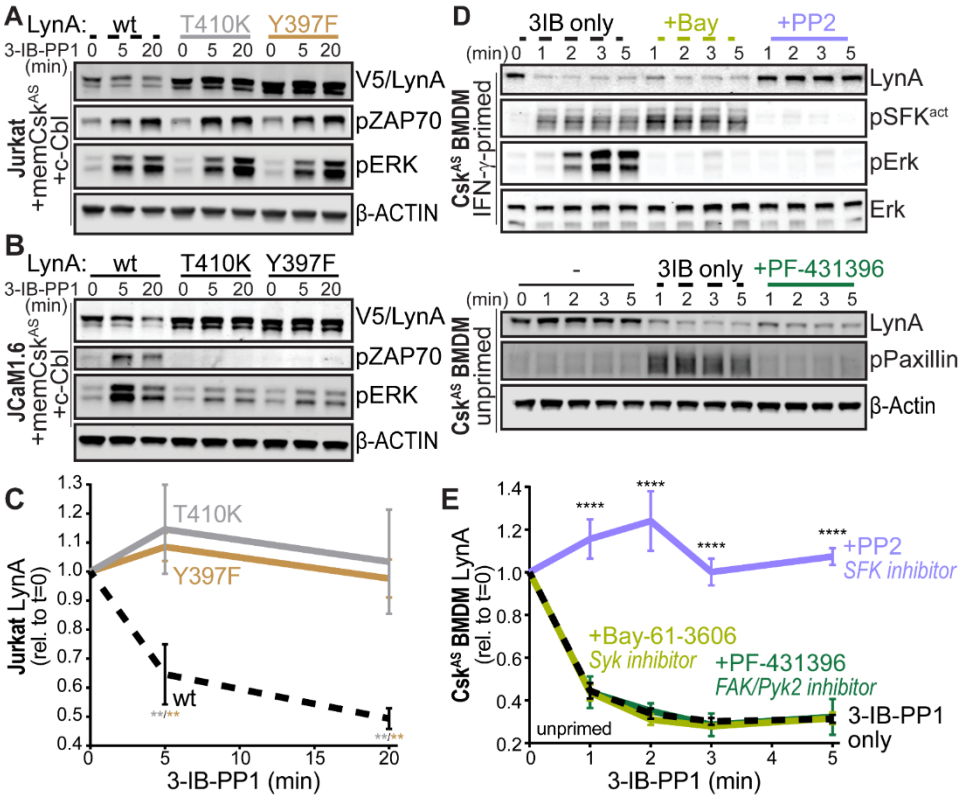

200

201 **Figure 4. SFK catalytic activity is required for rapid degradation of LynA. (A)** Immunoblots

202 showing ectopic expression of wild-type (wt, black dotted), substrate-binding-impaired (T410K, gray), or

203 activation-loop-mutated (Y397F, orange) V5-tagged LynA protein coexpressed in Jurkat cells with

204 memCsk^{AS} and c-Cbl and treated with 3-IB-PP1. pERK is shown as a control for 3-IB-PP1 treatment. β-

205 actin reflects lane loading. **(B)** Overexpression of wt and variants of LynA in JCaM1.6 cells. ZAP70

206 (Y319) and ERK are phosphorylated as a consequence of SFK activation. **(C)** Quantification of LynA

207 protein in transfected Jurkat cells during 3-IB-PP1 treatment, corrected for total protein, relative to the

208 steady-state level for each variant. SEM, n=3. Sig. from two-way ANOVA with Tukey's multiple

209 comparison test: [T410K vs. wt, gray asterisks], [Y397F vs. wt, orange asterisks]; ** P=0.0015-0.0083.

210 Other pairs ns. **(D)** Immunoblots showing expression of endogenous LynA protein in Csk^{AS} BMDMs

211 treated with 3-IB-PP1 (3IB only, black dotted) or with 3-IB-PP1 plus the Syk inhibitor Bay-61-3606 (Bay,

212 light olive), the SFK inhibitor PP2 (light purple), or the FAK/Pyk2 inhibitor PF-431396 (green).

213 Phosphorylated SFK activation loop Tyr416 (pSFK^{act}), Erk1/2 (pErk), and Paxillin Tyr118 (pPaxillin) are
214 shown as controls for inhibitor function; β-actin and Erk are shown as loading controls. **(E)**
215 Quantification of LynA protein during 3-IB-PP1 treatment, corrected for total protein, relative to the
216 steady-state level. SEM, n=3. Sig. from two-way ANOVA with Tukey's multiple comparison test: [+PP2
217 vs. 3IB only, asterisks]; **** P<0.0001. Other pairs ns. Refer to Figure 4–Source Data 1.

218 In untransfected Jurkat cells ERK1/2 is phosphorylated downstream of the endogenous SFKs Lck (43,
219 44) and Fyn (45), which are activated following treatment with 3-IB-PP1 (25). Since the endogenous
220 kinases are not disrupted by substitutions in transfected LynA, ERK1/2 continues to be efficiently
221 phosphorylated in cells transfected with LynA T410K or Y397F **(Figure 4A)**. In JCaM1.6 cells, an Lck-
222 deficient Jurkat strain (43, 46), ERK1/2 phosphorylation depended on transfected LynA and reflected
223 the functional impairment of LynA T410K and Y397F **(Figure 4B)**. As reported previously, Fyn activity
224 in the absence of Lck cannot mediate ERK1/2 phosphorylation (43).

225 Functional LynA kinase was required for c-Cbl-mediated degradation in Jurkat cells. While wild-type
226 LynA protein was 50% depleted after 20 min of 3-IB-PP1 treatment, degradation of either LynA T410K
227 or Y397F was undetectable **(Figure 4C)**. The dependence on LynA kinase function was evident in both
228 Lck- and Fyn-expressing Jurkat cells **(Figure 4A)** and Lck-deficient JCaM1.6 cells **(Figure 4B)**,
229 indicating that, in this system, the other activated SFKs could not target LynA in trans to induce c-Cbl-
230 mediated degradation. We do not yet know whether the unique insert of LynA is a substrate for the
231 other macrophage SFKs, but the peptide containing Tyr32 is a predicted SFK substrate (NetPhos 3.1,
232 38).

233 In macrophages and other hematopoietic cells the SFKs are the first kinases to be activated upon
234 antigen receptor engagement, phosphorylating intracellular ITAMs, ITAM-associated Syk or Zap70, and
235 integrin-associated FAK or Pyk2 (4, 47). We have reported that Syk and FAK are phosphorylated on
236 activating tyrosine residues in Csk^{AS} BMDMs treated with 3-IB-PP1 (20). To test whether these
237 downstream kinases might participate in negative feedback leading to LynA degradation, we treated

238 Csk^{AS} macrophages with competitive inhibitors of Syk (48), FAK/Pyk2 (49), or the SFKs themselves
239 (50) in combination with 3-IB-PP1. As controls for on-target effects, we demonstrated that Erk1/2 and
240 SFK activation-loop phosphorylation was blocked in samples cotreated with the pan-SFK inhibitor PP2,
241 that Erk1/2 but not SFK activation-loop phosphorylation was blocked in samples cotreated with the Syk
242 inhibitor BAY-61-3606, and that Paxillin phosphorylation was blocked in samples cotreated with the
243 FAK/Pyk2 inhibitor PF-431396 **(Figure 4D)**. As with genetically impairing LynA kinase function,
244 inhibiting SFK activity with PP2 abrogated LynA degradation **(Figure 4D-E)**. In contrast, LynA
245 degradation in BMDMs was unaffected by cotreatment with BAY-61-3606 or PF-431396. Together
246 these data suggest that Syk and FAK/Pyk2 (and any off-target effects of BAY-61-3606 and PF-431396)
247 do not participate in a larger negative-feedback process, suggesting that LynA might target itself
248 directly through Tyr32 in cis or trans. Interestingly, since the T-cell SFKs Lck and Fyn cannot effect
249 LynA degradation in trans, this feedback process could be limited to a kinase effect in cis or to another
250 macrophage-expressed Src family member. This tight feedback circuit could explain the strikingly fast
251 kinetics of LynA degradation.

252 **Differential Cbl expression tunes LynA protein levels and signaling responses in macrophages**
253 **and mast cells**

254 Analysis of data from the Immunological Genome Project shows that expression levels of Lyn and c-Cbl
255 RNA are differentially regulated across different cell types. Mast cells, for instance, express very low
256 levels of c-Cbl mRNA **(Figure 5)** (51, 52), which corresponds to a low level of c-Cbl protein expression
257 (53). Cbl-b mRNA, in contrast, is abundant in mast cells.

258 As in macrophages, Lyn is a key regulator of mast-cell ITAM signaling (54), but the effect of disparate
259 Cbl-family expression on LynA in the two cell types remains unknown. We generated bone-marrow-
260 derived mast cells from Csk^{AS} mice (hereafter referred to as “mast cells”) and performed surface marker
261 analysis as we had done already for BMDMs (20). Csk^{AS} mast cells were homogenous in their
262 expression of traditional mast-cell markers FcεR1α and c-Kit (CD117) (55) **(Figure 6A)**.

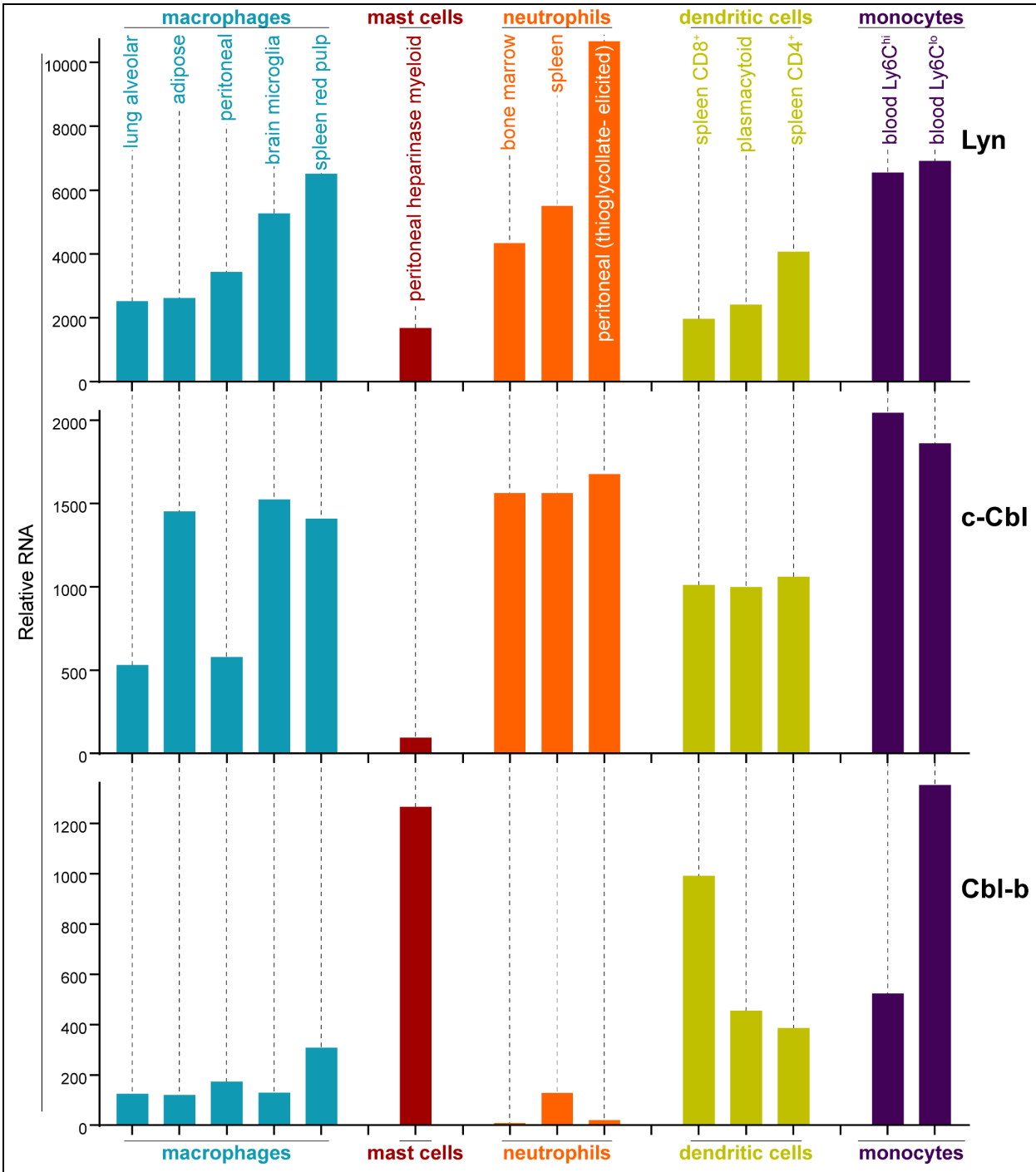

Figure 5. LynA, c-Cbl, and Cbl-b mRNAs are regulated differentially in myeloid cells. Mouse RNAseq data were derived from the Immunological Genome Project (ImmGen, http://rstats.immgen.org/Skyline/skyline.html, 51, 52). RNA levels of Lyn, c-Cbl, and Cbl-b are shown for macrophages, mast cells, neutrophils, dendritic cells, and blood monocytes. Refer to Figure 5–Source Data 1.

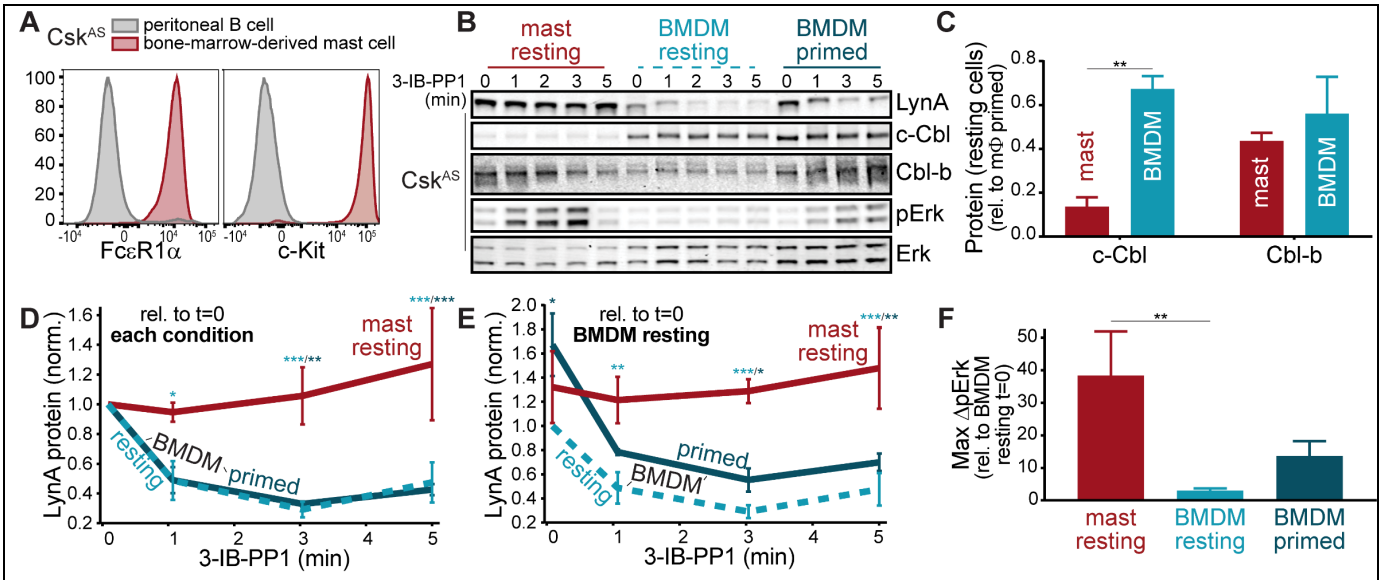

Figure 6. c-Cbl expression correlates with LynA protein levels and pathway activation in macrophages and mast cells. (A) Flow cytometry plots showing surface expression of the mast-cell markers FcεR1α and c-Kit (CD117) in Csk^{AS} bone-marrow-derived mast cells compared to a peritoneal B-cell control. **(B)** Immunoblots of Csk^{AS} bone-marrow-derived mast cells (mast resting, red) and BMDMs after resting (light teal) or IFN-γ priming (dark teal). LynA, c-Cbl, Cbl-b, and pErk1/2 are shown; total Erk1/2 reflects lane loading. **(C)** Quantification of c-Cbl and Cbl-b protein in mast cells and macrophages, corrected for total protein, relative to the level in primed macrophages (mΦ). SEM, n=3. Sig. from one-way ANOVA with Sidak multiple comparison test: [mast vs. BMDM resting, asterisk]; ** P= 0.0035. Others pairs ns. **(D-E)** Quantification of LynA, corrected for total protein, relative to the steady-state level in each cell condition **(D)** or in resting BMDMs at t=0 **(E)**. SEM, n=3 for mast cells and primed BMDMs, 4 for resting BMDMs. Sig. from two-way ANOVA with Tukey's multiple comparison test: [mast vs. BMDM resting, light teal asterisks], [mast vs. BMDM primed, dark teal asterisks]; *** P=0.0004-0.0008, ** P=0.0025-0.0088, * P=0.0134-0.0466. Other pairs ns. **(F)** Quantification of the maximum increase in pErk1/2 over the first 5 min of 3-IB-PP1 treatment, corrected for total Erk1/2 protein, relative to the level in resting BMDMs at t=0. SEM, n=3 for mast cells, 5 for resting BMDMs, and 4 for primed BMDMs. Sig. from one-way ANOVA with Tukey's multiple comparison test: [mast vs. BMDM resting, light teal asterisks]; ** P= 0.0085. Others pairs ns. Refer to Figure 6–Source Data 1.

287 We then used immunoblotting to compare the expression of Cbl and LynA protein in Csk^{AS} mast cells
288 and BMDMs **(Figure 6B)** and found that mast cells express very little c-Cbl (20% of the level in resting
289 macrophages) and relatively high levels of Cbl-b (80% of the level in resting macrophages) **(Figure**
290 **6C)**. Strikingly, low c-Cbl expression was accompanied by a complete resistance of LynA to
291 degradation in the first 5 min of 3-IB-PP1 treatment **(Figure 6D)** and an increase in steady-state
292 expression of LynA (30% higher than in resting BMDMs) **(Figure 6E)**, resulting in 3-4x more LynA
293 protein in mast cells than in resting BMDMs and 2x more than in primed BMDMs between 3 and 5 min
294 of 3-IB-PP1 treatment. Mast cells also had a stronger signaling response to 3-IB-PP1. Although the
295 kinetics of Erk phosphorylation in mast cells varied among experiments, the fold increase in pErk1/2 in
296 the first 5 min of 3-IB-PP1 treatment was consistently higher than in macrophages, even primed
297 BMDMs (40x pErk increase in mast cells compared with 14x in primed BMDMs and no significant
298 increase in resting BMDMs) **(Figure 6F)**. We therefore conclude that c-Cbl expression tunes the
299 steady-state expression of LynA protein and the cell's ability to target LynA for rapid degradation upon
300 activation. Since mast cells are less dependent on c-Cbl for positive signaling, long-lived LynA
301 potentiates a strong response to 3-IB-PP1. Thus mast cells bypass the LynA signaling checkpoint by
302 maintaining low levels of c-Cbl and therefore high levels of activated LynA.

303 Discussion

304 Both c-Cbl and Cbl-b negatively regulate ITAM signaling, recognizing activated signaling proteins via
305 PTB binding to activating phosphotyrosine sites. Cbl-mediated polyubiquitination leads to protein
306 degradation via the lysosome and proteasome (56). Cbl-family ligases must in turn be tightly regulated
307 to prevent hyperresponsive or aberrant signaling while maintaining proper pathogen clearance (57).
308 Although highly homologous, c-Cbl and Cbl-b target different subsets of signaling proteins for
309 degradation (58, 59), with c-Cbl targeting the SFKs, including Lyn (60, 61), and Cbl-b interacting with
310 ITAM-coupled receptors and other kinases (31, 53, 57). c-Cbl is thought to interact with active SFKs
311 through the SFK activation-loop phosphotyrosine residue, which binds the c-Cbl PTB domain (62), and
312 through the SFK SH3 domain, which binds the c-Cbl PXXP motifs (63). In this paper we report a new

313 mode of recognition specific to LynA. Although LynA and LynB have identical activation kinetics and
314 activation-loop and SH3-domain sequences, LynB is degraded 10-fold more slowly in macrophages
315 treated with 3-IB-PP1 (20). This rapid degradation profile is unique among the SFKs we have tested
316 (LynB, HckA, HckB, Fgr (20), and Fyn in BMDMs and Lck and Fyn in Jurkat cells). By exploiting the
317 similarity between LynA and LynB, we conclude that, while activation-loop phosphorylation and SH3-
318 domain interactions mediate slower-phase targeting by c-Cbl and other E3 ligases, rapid degradation of
319 LynA is triggered by an interaction unique to its insert region.

320 A single tyrosine residue (Tyr32) peculiar to its unique region marks activated LynA for rapid
321 degradation. This phenomenon is easily observed upon bulk SFK activation by 3-IB-PP1 but also
322 affects the steady-state level of LynA protein, likely due to the degradation of basally active LynA over
323 time. Phosphorylation of LynA Tyr32 has been observed in neuroblastoma cell lines upon receptor-
324 tyrosine-kinase activation (64). Further, in epidermoid carcinoma (A431) cells and breast tumor
325 samples LynA Tyr32 is phosphorylated by the epidermal growth factor receptor (EGFR), allowing it to
326 phosphorylate MCM-7 and stimulate cell proliferation (36). In macrophages this potentially positive-
327 regulatory function of Tyr32 paradoxically causes LynA to trigger its own c-Cbl-mediated degradation,
328 underlying its function as a rheostat in the LynA checkpoint. We can speculate about two possible
329 mechanisms. First, by analogy to a similarly situated but non-homologous transautophosphorylation
330 site in Hck (Tyr^{29}) (65), LynA phospho-Tyr32 may be directly activating. The unique regions of LynA
331 and LynB make distinct SH3-domain contacts (66), and phospho-Tyr32 could alter these interactions.
332 Hyperactivated LynA could then efficiently phosphorylate and activate nearby or pre-complexed c-Cbl,
333 triggering its own degradation more aggressively than do the other SFKs. Alternatively, phospho-Tyr32
334 could directly or indirectly serve as a docking site for c-Cbl, constituting a unique interaction site to
335 efficiently recruit its degradation machinery. Bolstering this hypothesis is a published study showing that
336 the interactome of $LynA^{Y32F}$ transfected into mammary adenocarcinoma (MDA-MB-231) cells more
337 closely resembles the interactome of wild-type LynA than LynB, but some LynA interactions are lost
338 (67). It is also possible that LynA Tyr32 is not phosphorylated, but is required for an allosteric

339 intramolecular interaction or docking of interacting proteins.

340 We have shown that SFK activity is required for LynA degradation, and LynA Tyr32 is a predicted
341 substrate for Hck (NetPhos 3.1, 38) in addition to EGFR. It is therefore tempting to speculate that LynA
342 Tyr32 is a site of autophosphorylation, since the SFKs Lck and Fyn cannot mediate the degradation of
343 kinase-impaired LynA in trans. On the other hand, we have shown that LynA and LynB are activation-
344 loop phosphorylated 20x more quickly than Hck and Fgr in response to 3-IB-PP1 (20), and it is possible
345 that this delay could function as a timer, allowing a rapid burst of LynA activation with a short half-life,
346 either globally (in the case of 3-IB-PP1 treatment) or at the single-molecule scale within a phagocytic
347 synapse.

348 LynA and LynB have been reported to interact with different subsets of proteins in mast cells and in
349 triple-negative breast cancer cells, with LynA signaling via ITAM (18), cytoskeletal, and proliferative (67)
350 pathways and LynB initiating negative feedback via ITIMs and phosphatases (18). In mammary
351 epithelial cells the ratio of LynA and LynB is actively regulated by Epithelial Splicing Regulatory Protein
352 1 (ESRP1), with LynA-upregulated tumors having the more invasive phenotype (67). The positive-
353 regulatory roles reported for LynA in mast and tumor cells complements our own observations that
354 LynA degradation can block macrophage signaling through the Erk, Akt, and NFAT pathways, which
355 cannot be complemented by active LynB (20).

356 Aberrant activation driven by ITAM signaling pathways in macrophages is a known driver of
357 autoimmune and inflammatory disease, with activated macrophages accumulating in chronically
358 inflamed tissues in the absence of an active infection (68). Regulation of LynA protein expression and
359 deactivation kinetics by c-Cbl, could, via the LynA checkpoint, help to prevent the initiation of
360 pathological signaling. The threshold for macrophage activation is modifiable by changes to their local
361 environment. For example, IFN-γ and LPS polarize macrophages for a pro-inflammatory response,
362 whereas IL-4 and IL-13 polarize macrophages for tissue repair (i.e. collagen deposition) and
363 inflammatory resolution (69, 70). We have reported that IFN-γ decreases the macrophage signaling

364 threshold in part by increasing the expression of LynA (20). Dynamic changes in SFK and c-Cbl levels
365 could modulate the macrophage activation threshold, ensuring that macrophages respond appropriately
366 during times of infection (low threshold) and limiting aberrant activation in response to cellular debris
367 and small-scale antibody complexes during inflammatory resolution (high threshold).

368 Like macrophages, mast cells reside in nearly every bodily tissue and perform environment-specific
369 functions in addition to sensing non-self (69, 71). While macrophages have distinct anti-inflammatory
370 roles as professional phagocytes in the silent clearance of apoptotic cells and agents of wound healing,
371 mast cells are constitutively primed for ITAM-induced triggering, releasing preformed granules that
372 contain inflammatory cytokines, chemokines, prostaglandins, and proteases. Pursuant to these differing
373 functions, macrophages continuously gauge ITAM ligand valency (*i.e.* particle size) and have a
374 relatively high basal threshold for inflammatory activation (5, 20), while mast cells can be triggered by
375 small-scale receptor clustering induced by low-valency or even monovalent FcεR-IgE-allergen
376 complexes (21, 22). One striking difference between the macrophage and mast-cell ITAM regulatory
377 machinery is that mast cells express almost no c-Cbl. In spite of low reported mRNA levels (ImmGen,
378 51, 52), mast cells constitutively express a high level of LynA protein, likely due to impaired steady-
379 state degradation of basally active LynA. Furthermore, LynA is not degraded upon activation and 3-IB-
380 PP1 triggers a stronger Erk phosphorylation response in the absence of ITAM-receptor ligation in
381 resting mast cells than in resting macrophages.

382 Overall, we describe a model in which regulation of LynA and c-Cbl levels helps to determine an
383 immune cell's potential for inflammatory ITAM signaling. Regulated degradation tunes down the LynA
384 rheostat, blocking cell signaling via the LynA checkpoint at low cellular doses of LynA and overriding
385 the LynA checkpoint at higher doses. In macrophages, this occurs on a continuum where LynA dose is
386 highest in M1-polarized cells but still susceptible to rapid degradation by c-Cbl. Mast cells express
387 almost no c-Cbl and maintain high levels of LynA at steady state and over time, consistent with
388 permissive signaling in the absence of large-scale ITAM receptor clustering nucleated by multivalent
389 receptor ligation. Appropriate regulation of immune receptor thresholds is critical for maintaining the

390 function of innate immune cells; threshold dysregulation can lead to chronic feedback loops that drive
391 inflammatory signaling in autoimmune disease and conversely tumor-supporting immunosuppressive
392 signaling (68). Elucidating the mechanisms by which the LynA checkpoint is regulated may allow us to
393 tune immune-cell sensitivity and reprogram pathological cells without causing immunodeficiency.

394 Materials and Methods

395 Mice

396 C57BL/6-derived *Csk*^{AS} mice are hemizygous for the *Csk*^{AS} BAC transgene on a *Csk*$^{-/-}$ background, as
397 described previously (20, 26). Due to sterility of c-Cbl$^{-/-}$ male mice, we were not able to produce a
398 sustained lineage of *Csk*^{AS}*Cbl*$^{-/-}$ mice, but we obtained three individuals by crossing *c-Cbl*$^{-/-}$ female mice
399 from E. Peterson (University of Minnesota) (72) with *Csk*$^{+/-}$ (26) and *Csk*^{AS} male mice from our colony
400 and then crossing *Cbl*$^{+/-}$*Csk*$^{+/-}$ *with Cbl*$^{+/-}$*Csk*^{AS} mice. All mice were housed in specific pathogen-free
401 conditions and genotyped using real-time PCR (Transnetyx, Inc., Memphis, TN).

402 Jurkat cell lines and transfection

403 The Jurkat T-cell strains E6-1 ("wild-type") (73) and JCaM1.6 (Lck-deficient) (43, 46) were gifts from the
404 laboratories of A. Weiss (University of California, San Francisco) and Y. Shimizu (University of
405 Minnesota), respectively. Jurkat cell lines were cultured in RPMI-1640 medium supplemented with 5%
406 fetal calf serum (Omega Scientific, Inc., Tarzana, CA) and 2 mM glutamine, penicillin and streptomycin
407 (Sigma-Aldrich, St. Louis, MO) as described previously *(74).* Jurkat and JCaM1.6 cells were transiently
408 transfected via electroporation, as described previously (74). Briefly, cells were grown overnight in
409 antibiotic-free RPMI-1640 medium supplemented with 10% fetal bovine serum (Omega Scientific) and 2
410 mM glutamine (RPMI10). Batches of 15 M cells were resuspended in RPMI10 with 15 µg plasmid DNA
411 per construct. Cells were rested 20 min, electroporated 285 V/10 ms in a BTX square-wave
412 electroporator (Harvard Apparatus, Holliston, MA), resuspended in 10 mL RPMI10, and allowed to
413 recover overnight. One million live cells were then resuspended in phosphate-buffered saline, rested for

414 30 min at 37°C, and stimulated.

415 **DNA constructs and mutagenesis**

416 Plasmids containing V5+His-tagged mouse LynA and LynB were gifts from J. Rivera/R. Suzuki
417 (National Institutes of Health) (18). Myc-tagged mouse memCsk^{AS} (also referred to as Lck$_{11}$-Csk^{AS}) (25)
418 and Xpress-tagged human c-Cbl and Cbl-b (75) were gifts from A. Weiss (University of California, San
419 Francisco). Site-directed mutagenesis was performed using QuikChange Lightning (Agilent
420 Technologies, Santa Clara, CA). Sequences of all constructs were verified by Sanger sequencing
421 (GENEWIZ, South Plainfield, NJ).

422 **Preparation and flow cytometry of myeloid cells**

423 BMDMs were prepared using standard methods (76). Briefly, bone marrow was extracted from femura
424 and tibiae of mice aged 6-8-weeks. After hypotonic lysis of erythrocytes, BMDMs were derived on
425 untreated plastic plates (BD Falcon, Sigma-Aldrich) by culturing in Dulbecco's Modified Eagle Medium
426 (DMEM, Corning Cellgro, Corning, NY) containing approximately 10% heat-inactivated fetal calf serum
427 (Omega Scientific), 0.11 mg/ml sodium pyruvate (Corning), 2 mM penicillin/streptomycin/L-glutamine
428 (Sigma-Aldrich), and 10% CMG-14-12-cell-conditioned medium as a source of M-CSF (77). After 6 or 7
429 days cells were resuspended in enzyme-free EDTA buffer and replated in untreated 6-well plates (BD
430 Falcon, Sigma-Aldrich) at 1 M cells per well in unconditioned medium with or without priming in 25 U
431 IFN-γ (PeproTech, Rocky Hill, NJ). Bone-marrow-derived mast cells were prepared as described
432 previously (55), as above except for the substitution of 10 ng/ml IL-3 (PeproTech) for CMG-14-12-
433 conditoned medium. After 5 weeks, cells were subjected to flow-cytometry analysis (LSRFortessa,
434 Becton Dickinson, Franklin Lakes, NJ) and found to be uniformly positive for FcεRIα (Mar-1, FITC-
435 labeled, #134305) and c-Kit (2B8, APC-labeled, #105811), both from BioLegend (San Diego, CA). Cells
436 were rested or primed overnight before stimulation.

437 **siRNA knockdown**

438 The siRNA sequence for knockdown of mouse c-Cbl was adapted from human siRNA. Cbl-b siRNA
439 was designed using the Integrated DNA Technologies double-stranded siRNA design tools (IDT,
440 Skokie, IL). Control double-stranded RNA from IDT was not predicted to be complementary to any
441 sequence in human, mouse, or rat transcriptomes. 2 M BMDMs in 100 μL opti-MEM (ThermoFisher,
442 Waltham, MA) were transfected with 1 μM siRNA via electroporation at 400 V/10 ms using a BTX
443 square-wave electroporator. Cells were then plated on 150 mm untreated cell culture dishes and rested
444 in 10 mL DMEM-10 for 30 min before adding 10 mL DMEM-10 supplemented with 10% CMG-14-12-
445 cell-conditioned medium as a source of M-CSF. Transfections were pooled from several cuvettes to
446 obtain enough cells for several stimulation conditions. After 24 h cells were resuspended in enzyme-
447 free EDTA buffer and replated in untreated 6-well plates (BD Falcon, Sigma-Aldrich) at 1 M cells per
448 well in unconditioned medium. Cells were used 48 h after transfection.

449 **Cell stimulation**

450 BMDM stimulations have been described previously (20). After resting as described above, 1 M live
451 Jurkat cells, mast cells, or adherent BMDMs were treated at 37°C in DMEM (myeloid cells) or PBS
452 (Jurkat cells) with 10 μM 3-IB-PP1, a gift from K. Shokat (University of California, San Francisco).
453 Signaling reactions were quenched by placing on ice and lysing cells in sodium dodecyl sulfate (SDS)
454 buffer (128 mM Tris base, 10% glycerol, 4% SDS, 50 mM dithiothreitol, pH 6.8). Whole-cell lysates
455 were prepared for immunoblotting by sonicating with a Bioruptor (Diagenode, Inc., Denville, NJ) for 3
456 min and boiling for 15 min.

457 **Antibodies and immunoblotting**

458 After sample preparation, 0.25 M cell equivalents were run on each lane of a 7% NuPage Tris-Acetate
459 gel (Invitrogen, Carlsbad, CA) and then transferred to an Immobilon-FL PVDF membrane (EMD
460 Millipore, Burlington, MA). REVERT Total Protein Stain was used according to the standard protocol to
461 quantify lane loading. After destaining, membranes were then treated with Odyssey® Blocking Buffer
462 (TBS) for at least 1 h. Blotting was performed using standard procedures, and blots were imaged on an

463 Odyssey CLx near-infrared imager (LI-COR Biosciences, Lincoln, NE). Antibodies for immunoblotting
464 were purchased from Cell Signaling Technology (Danvers, MA), ProMab Biotechnologies (Richmond,
465 CA), Thermo Fisher Scientific (Waltham, MA), LifeSpan Biosciences (Seattle, WA), Abcam (Cambridge,
466 UK), and LI-COR Biosciences as follows:

Antibody	Source and Catalog No.
β-Actin (8H10D10)	Cell Signaling 3700
c-Cbl (D4E10)	Cell Signaling 8447
Cbl-b (D3C12)	Cell Signaling 9498
pErk1/2 (phosphoThr^{202}/phosphoTyr^{204}, D13.14.4E)	Cell Signaling 4370
Erk1/2 (3A7)	Cell Signaling 9107
Fyn	Cell Signaling 4023
Lck (D88) XP(R)	Cell Signaling 2984
LynA (C13F9)	Cell Signaling 2796
LynA + LynB (Lyn-01)	Abcam ab1890
Myc (9B11)	Cell Signaling 2276
pPaxillin (phosphoTyr^{118})	Cell Signaling 2541
pSFK^{act} (phosphoTyr^{416})	Cell Signaling 2101
pZAP70/pSyk (phosphoTyr$^{319(Zap)/352(Syk)}$, 65E4)	Cell Signaling 2717
V5 (D3H8Q)	Cell Signaling 13202
Donkey anti-rabbit IgG 800CW	LI-COR 925-32213
Donkey anti-rabbit IgG 680LT	LI-COR 925-68023
Donkey anti-mouse IgG 800CW	LI-COR 925-32212
Donkey anti-mouse IgG 680LT	LI-COR 925-68022

467 **Quantification, statistics, and image processing**

468 Immunoblots were analyzed by densitometry from ImageStudio software (LI-COR Biosciences). Images
469 were background-subtracted, and bands of the appropriate molecular weight were demarcated and
470 analyzed for each gel lane. Each value was corrected for the total lane protein content (REVERT stain,
471 above). Data were further normalized to a control condition to show relative changes in protein content.
472 Where phosphoproteins were quantified, these were corrected for the total amount of the individual
473 protein, rather than whole-lane protein content. For all figures, n values are biological replicates,
474 reflecting independent experiments from different batches of cells, stimulus preparations, and
475 experimental workflows. Statistical analyses were performed using Prism Software (Graphpad, La Jolla,
476 CA). Significance was assessed using one- or two-way ANOVA analysis with Tukey's or Sidak
477 correction for multiple comparisons as indicated in the figure legends, with analysis of the mean at each
478 time point or condition. Error bars in each figure represent standard errors of the mean from at least

479 three independent experiments. Asterisks reflect specified P-values. Figures were further prepared
480 using Adobe Creative Cloud software (San Jose, CA). Where appropriate, images were optimized by
481 applying brightness/contrast changes to the whole image. No gamma correction was used. Images
482 were only rotated after densitometry analysis was completed.

483 References

484 1. Guilliams M, Bruhns P, Saeys Y, Hammad H, Lambrecht BN. The function of Fcgamma
485 receptors in dendritic cells and macrophages. Nat Rev Immunol. 2014;14(2):94-108.

486 2. Brown GD. Dectin-1: a signalling non-TLR pattern-recognition receptor. Nat Rev Immunol.
487 2006;6(1):33-43.

488 3. Deng Z, Ma S, Zhou H, Zang A, Fang Y, Li T, et al. Tyrosine phosphatase SHP-2 mediates C-
489 type lectin receptor-induced activation of the kinase Syk and anti-fungal TH17 responses. Nat Immunol.
490 2015;16(6):642-52.

491 4. Lowell CA. Src-family and Syk kinases in activating and inhibitory pathways in innate immune
492 cells: signaling cross talk. Cold Spring Harb Perspect Biol. 2011;3(3).

493 5. Goodridge HS, Reyes CN, Becker CA, Katsumoto TR, Ma J, Wolf AJ, et al. Activation of the
494 innate immune receptor Dectin-1 upon formation of a 'phagocytic synapse'. Nature.
495 2011;472(7344):471-5.

496 6. Takai T. Roles of Fc receptors in autoimmunity. Nat Rev Immunol. 2002;2(8):580-92.

497 7. Sondermann P. The FcgammaR/IgG Interaction as Target for the Treatment of Autoimmune
498 Diseases. J Clin Immunol. 2016;36 Suppl 1:95-9.

499 8. Chiffoleau E. C-Type Lectin-Like Receptors As Emerging Orchestrators of Sterile Inflammation
500 Represent Potential Therapeutic Targets. Front Immunol. 2018;9:227.

501 9. Freeman SA, Goyette J, Furuya W, Woods EC, Bertozzi CR, Bergmeier W, et al. Integrins Form
502 an Expanding Diffusional Barrier that Coordinates Phagocytosis. Cell. 2016;164(1-2):128-40.

503 10. Bakalar MH, Joffe AM, Schmid EM, Son S, Podolski M, Fletcher DA. Size-Dependent
504 Segregation Controls Macrophage Phagocytosis of Antibody-Opsonized Targets. Cell.
505 2018;174(1):131-42 e13.

506 11. Jaumouille V, Farkash Y, Jaqaman K, Das R, Lowell CA, Grinstein S. Actin cytoskeleton
507 reorganization by Syk regulates Fcgamma receptor responsiveness by increasing its lateral mobility
508 and clustering. Dev Cell. 2014;29(5):534-46.

509 12. Abram CL, Lowell CA. The diverse functions of Src family kinases in macrophages. Front
510 Biosci. 2008;13:4426-50.

511 13. Hamerman JA, Lanier LL. Inhibition of immune responses by ITAM-bearing receptors. Sci
512 STKE. 2006;2006(320):re1.

513 14. Hamerman JA, Ni M, Killebrew JR, Chu CL, Lowell CA. The expanding roles of ITAM adapters
514 FcRgamma and DAP12 in myeloid cells. Immunol Rev. 2009;232(1):42-58.

515 15. Lutz-Nicoladoni C, Wolf D, Sopper S. Modulation of Immune Cell Functions by the E3 Ligase
516 Cbl-b. Front Oncol. 2015;5:58.

517 16. Liyasova MS, Ma K, Lipkowitz S. Molecular pathways: cbl proteins in tumorigenesis and
518 antitumor immunity-opportunities for cancer treatment. Clin Cancer Res. 2015;21(8):1789-94.

519 17. Mkaddem SB, Murua A, Flament H, Titeca-Beauport D, Bounaix C, Danelli L, et al. Lyn and Fyn
520 function as molecular switches that control immunoreceptors to direct homeostasis or inflammation. Nat
521 Commun. 2017;8(1):246.

522 18. Alvarez-Errico D, Yamashita Y, Suzuki R, Odom S, Furumoto Y, Yamashita T, et al. Functional
523 analysis of Lyn kinase A and B isoforms reveals redundant and distinct roles in Fc epsilon RI-
524 dependent mast cell activation. J Immunol. 2010;184(9):5000-8.

525 19. Scapini P, Pereira S, Zhang H, Lowell CA. Multiple roles of Lyn kinase in myeloid cell signaling
526 and function. Immunol Rev. 2009;228(1):23-40.

527 20. Freedman TS, Tan YX, Skrzypczynska KM, Manz BN, Sjaastad FV, Goodridge HS, et al. LynA
528 regulates an inflammation-sensitive signaling checkpoint in macrophages. Elife. 2015;4.

529 21. Andrews NL, Pfeiffer JR, Martinez AM, Haaland DM, Davis RW, Kawakami T, et al. Small,
530 mobile FcepsilonRI receptor aggregates are signaling competent. Immunity. 2009;31(3):469-79.

531 22. Felce JH, Sezgin E, Wane M, Brouwer H, Dustin ML, Eggeling C, et al. CD45 exclusion- and
532 cross-linking-based receptor signaling together broaden FcepsilonRI reactivity. Sci Signal.
533 2018;11(561).

534 23. Okuzumi T, Ducker GS, Zhang C, Aizenstein B, Hoffman R, Shokat KM. Synthesis and
535 evaluation of indazole based analog sensitive Akt inhibitors. Mol Biosyst. 2010;6(8):1389-402.

536 24. Okuzumi T, Fiedler D, Zhang C, Gray DC, Aizenstein B, Hoffman R, et al. Inhibitor hijacking of
537 Akt activation. Nat Chem Biol. 2009;5(7):484-93.

538 25. Schoenborn JR, Tan YX, Zhang C, Shokat KM, Weiss A. Feedback circuits monitor and adjust
539 basal Lck-dependent events in T cell receptor signaling. Sci Signal. 2011;4(190):ra59.

540 26. Tan YX, Manz BN, Freedman TS, Zhang C, Shokat KM, Weiss A. Inhibition of the kinase Csk in
541 thymocytes reveals a requirement for actin remodeling in the initiation of full TCR signaling. Nat
542 Immunol. 2014;15(2):186-94.

543 27. Chow LM, Veillette A. The Src and Csk families of tyrosine protein kinases in hemopoietic cells.
544 Semin Immunol. 1995;7(4):207-26.

545 28. Zhu JW, Doan K, Park J, Chau AH, Zhang H, Lowell CA, et al. Receptor-like tyrosine
546 phosphatases CD45 and CD148 have distinct functions in chemoattractant-mediated neutrophil
547 migration and response to S. aureus. Immunity. 2011;35(5):757-69.

548 29. Tang R, Langdon WY, Zhang J. Regulation of immune responses by E3 ubiquitin ligase Cbl-b.
549 Cell Immunol. 2018.

550 30. Naramura M, Jang IK, Kole H, Huang F, Haines D, Gu H. c-Cbl and Cbl-b regulate T cell
551 responsiveness by promoting ligand-induced TCR down-modulation. Nat Immunol. 2002;3(12):1192-9.

552 31. Purev E, Neff L, Horne WC, Baron R. c-Cbl and Cbl-b act redundantly to protect osteoclasts
553 from apoptosis and to displace HDAC6 from beta-tubulin, stabilizing microtubules and podosomes. Mol
554 Biol Cell. 2009;20(18):4021-30.

555 32. Ueno H, Sasaki K, Honda H, Nakamoto T, Yamagata T, Miyagawa K, et al. c-Cbl is tyrosine-
556 phosphorylated by interleukin-4 and enhances mitogenic and survival signals of interleukin-4 receptor
557 by linking with the phosphatidylinositol 3'-kinase pathway. Blood. 1998;91(1):46-53.

558 33. Hunter S, Burton EA, Wu SC, Anderson SM. Fyn associates with Cbl and phosphorylates
559 tyrosine 731 in Cbl, a binding site for phosphatidylinositol 3-kinase. J Biol Chem. 1999;274(4):2097-
560 106.

561 34. Yi TL, Bolen JB, Ihle JN. Hematopoietic cells express two forms of lyn kinase differing by 21
562 amino acids in the amino terminus. Mol Cell Biol. 1991;11(5):2391-8.

563 35. Stanley E, Ralph S, McEwen S, Boulet I, Holtzman DA, Lock P, et al. Alternatively spliced
564 murine lyn mRNAs encode distinct proteins. Mol Cell Biol. 1991;11(7):3399-406.

565 36. Huang TH, Huo L, Wang YN, Xia W, Wei Y, Chang SS, et al. Epidermal growth factor receptor
566 potentiates MCM7-mediated DNA replication through tyrosine phosphorylation of Lyn kinase in human
567 cancers. Cancer cell. 2013;23(6):796-810.

568 37. Radivojac P, Vacic V, Haynes C, Cocklin RR, Mohan A, Heyen JW, et al. Identification,
569 analysis, and prediction of protein ubiquitination sites. Proteins. 2010;78(2):365-80.

570 38. Blom N, Sicheritz-Ponten T, Gupta R, Gammeltoft S, Brunak S. Prediction of post-translational
571 glycosylation and phosphorylation of proteins from the amino acid sequence. Proteomics.
572 2004;4(6):1633-49.

573 39. Verhagen AM, Wallace ME, Goradia A, Jones SA, Croom HA, Metcalf D, et al. A kinase-dead
574 allele of Lyn attenuates autoimmune disease normally associated with Lyn deficiency. J Immunol.
575 2009;182(4):2020-9.

576 40. Yokoyama N, Miller WT. Identification of residues involved in v-Src substrate recognition by site-
577 directed mutagenesis. FEBS Lett. 1999;456(3):403-8.

578 41. Xu W, Doshi A, Lei M, Eck MJ, Harrison SC. Crystal structures of c-Src reveal features of its
579 autoinhibitory mechanism. Mol Cell. 1999;3(5):629-38.

580 42. Brown MT, Cooper JA. Regulation, substrates and functions of src. Biochim Biophys Acta.
581 1996;1287(2-3):121-49.

582 43. Straus DB, Weiss A. Genetic evidence for the involvement of the lck tyrosine kinase in signal
583 transduction through the T cell antigen receptor. Cell. 1992;70(4):585-93.

584 44. Burgess KE, Odysseos AD, Zalvan C, Druker BJ, Anderson P, Schlossman SF, et al.
585 Biochemical identification of a direct physical interaction between the CD4:p56lck and Ti(TcR)/CD3
586 complexes. Eur J Immunol. 1991;21(7):1663-8.

587 45. Samelson LE, Phillips AF, Luong ET, Klausner RD. Association of the fyn protein-tyrosine
588 kinase with the T-cell antigen receptor. Proc Natl Acad Sci U S A. 1990;87(11):4358-62.

589 46. Goldsmith MA, Weiss A. Isolation and characterization of a T-lymphocyte somatic mutant with
590 altered signal transduction by the antigen receptor. Proc Natl Acad Sci U S A. 1987;84(19):6879-83.

591 47. Han J, Zhang G, Welch EJ, Liang Y, Fu J, Vogel SM, et al. A critical role for Lyn kinase in
592 strengthening endothelial integrity and barrier function. Blood. 2013;122(25):4140-9.

593 48. Yamamoto N, Takeshita K, Shichijo M, Kokubo T, Sato M, Nakashima K, et al. The orally
594 available spleen tyrosine kinase inhibitor 2-[7-(3,4-dimethoxyphenyl)-imidazo[1,2-c]pyrimidin-5-
595 ylamino]nicotinamide dihydrochloride (BAY 61-3606) blocks antigen-induced airway inflammation in
596 rodents. The Journal of pharmacology and experimental therapeutics. 2003;306(3):1174-81.

597 49. Buckbinder L, Crawford DT, Qi H, Ke HZ, Olson LM, Long KR, et al. Proline-rich tyrosine kinase
598 2 regulates osteoprogenitor cells and bone formation, and offers an anabolic treatment approach for
599 osteoporosis. Proc Natl Acad Sci U S A. 2007;104(25):10619-24.

600 50. Hanke JH, Gardner JP, Dow RL, Changelian PS, Brissette WH, Weringer EJ, et al. Discovery of
601 a novel, potent, and Src family-selective tyrosine kinase inhibitor. Study of Lck- and FynT-dependent T
602 cell activation. J Biol Chem. 1996;271(2):695-701.

603 51. Heng TS, Painter MW, Immunological Genome Project C. The Immunological Genome Project:
604 networks of gene expression in immune cells. Nat Immunol. 2008;9(10):1091-4.

605 52. Dwyer DF, Barrett NA, Austen KF, Immunological Genome Project C. Expression profiling of
606 constitutive mast cells reveals a unique identity within the immune system. Nat Immunol.
607 2016;17(7):878-87.

608 53. Gustin SE, Thien CB, Langdon WY. Cbl-b is a negative regulator of inflammatory cytokines
609 produced by IgE-activated mast cells. J Immunol. 2006;177(9):5980-9.

610 54. Shelby SA, Veatch SL, Holowka DA, Baird BA. Functional nanoscale coupling of Lyn kinase
611 with IgE-FcepsilonRI is restricted by the actin cytoskeleton in early antigen-stimulated signaling. Mol
612 Biol Cell. 2016;27(22):3645-58.

613 55. Kalesnikoff J, Galli SJ. Antiinflammatory and immunosuppressive functions of mast cells.
614 Methods Mol Biol. 2011;677:207-20.

615 56. Duan L, Reddi AL, Ghosh A, Dimri M, Band H. The Cbl family and other ubiquitin ligases:
616 destructive forces in control of antigen receptor signaling. Immunity. 2004;21(1):7-17.

617 57. Zhu LL, Luo TM, Xu X, Guo YH, Zhao XQ, Wang TT, et al. E3 ubiquitin ligase Cbl-b negatively
618 regulates C-type lectin receptor-mediated antifungal innate immunity. J Exp Med. 2016;213(8):1555-70.

619 58. Thien CB, Langdon WY. c-Cbl and Cbl-b ubiquitin ligases: substrate diversity and the negative
620 regulation of signalling responses. Biochem J. 2005;391(Pt 2):153-66.

621 59. Mohapatra B, Ahmad G, Nadeau S, Zutshi N, An W, Scheffe S, et al. Protein tyrosine kinase
622 regulation by ubiquitination: critical roles of Cbl-family ubiquitin ligases. Biochim Biophys Acta.
623 2013;1833(1):122-39.

624 60. Kyo S, Sada K, Qu X, Maeno K, Miah SMS, Kawauchi-Kamata K, et al. Negative regulation of
625 Lyn protein-tyrosine kinase by c-Cbl ubiquitin-protein ligase in FceRI-mediated mast cell activation.
626 Genes to Cells. 2003;8(10):825-36.

627 61. Shao Y, Yang C, Elly C, Liu YC. Differential regulation of the B cell receptor-mediated signaling
628 by the E3 ubiquitin ligase Cbl. J Biol Chem. 2004;279(42):43646-53.

629 62. Sanjay A, Houghton A, Neff L, DiDomenico E, Bardelay C, Antoine E, et al. Cbl associates with
630 Pyk2 and Src to regulate Src kinase activity, alpha(v)beta(3) integrin-mediated signaling, cell adhesion,
631 and osteoclast motility. J Cell Biol. 2001;152(1):181-95.

632 63. Sanjay A, Miyazaki T, Itzstein C, Purev E, Horne WC, Baron R. Identification and functional
633 characterization of an Src homology domain 3 domain-binding site on Cbl. FEBS J. 2006;273(23):5442-
634 56.

635 64. Palacios-Moreno J, Foltz L, Guo A, Stokes MP, Kuehn ED, George L, et al. Neuroblastoma
636 tyrosine kinase signaling networks involve FYN and LYN in endosomes and lipid rafts. PLoS Comput
637 Biol. 2015;11(4):e1004130.

638 65. Johnson TM, Williamson NA, Scholz G, Jaworowski A, Wettenhall RE, Dunn AR, et al.
639 Modulation of the catalytic activity of the Src family tyrosine kinase Hck by autophosphorylation at a
640 novel site in the unique domain. J Biol Chem. 2000;275(43):33353-64.

641 66. Teixeira J, Fuentes H, Bielskutė S, Gairi M, Żerko S, Koźmiński W, et al. The Two Isoforms of
642 Lyn Display Different Intramolecular Fuzzy Complexes with the SH3 Domain. Molecules. 2018;23(11).

643 67. Tornillo G, Knowlson C, Kendrick H, Cooke J, Mirza H, Aurrekoetxea-Rodriguez I, et al. Dual
644 Mechanisms of LYN Kinase Dysregulation Drive Aggressive Behavior in Breast Cancer Cells. Cell Rep.
645 2018;25(13):3674-92 e10.

646 68. Wynn TA, Chawla A, Pollard JW. Macrophage biology in development, homeostasis and
647 disease. Nature. 2013;496(7446):445-55.

648 69. Galli SJ, Borregaard N, Wynn TA. Phenotypic and functional plasticity of cells of innate
649 immunity: macrophages, mast cells and neutrophils. Nat Immunol. 2011;12(11):1035-44.

650 70. Bosurgi L, Cao YG, Cabeza-Cabrerizo M, Tucci A, Hughes LD, Kong Y, et al. Macrophage
651 function in tissue repair and remodeling requires IL-4 or IL-13 with apoptotic cells. Science.
652 2017;356(6342):1072-6.

653 71. Gentek R, Ghigo C, Hoeffel G, Bulle MJ, Msallam R, Gautier G, et al. Hemogenic Endothelial
654 Fate Mapping Reveals Dual Developmental Origin of Mast Cells. Immunity. 2018;48(6):1160-71 e5.

655 72. Rafiq K, Kolpakov MA, Seqqat R, Guo J, Guo X, Qi Z, et al. c-Cbl inhibition improves cardiac
656 function and survival in response to myocardial ischemia. Circulation. 2014;129(20):2031-43.

657 73. Weiss A, Stobo JD. Requirement for the coexpression of T3 and the T cell antigen receptor on a
658 malignant human T cell line. J Exp Med. 1984;160(5):1284-99.

659 74. Phee H, Abraham RT, Weiss A. Dynamic recruitment of PAK1 to the immunological synapse is
660 mediated by PIX independently of SLP-76 and Vav1. Nat Immunol. 2005;6(6):608-17.

661 75. Myers MD, Sosinowski T, Dragone LL, White C, Band H, Gu H, et al. Src-like adaptor protein
662 regulates TCR expression on thymocytes by linking the ubiquitin ligase c-Cbl to the TCR complex. Nat
663 Immunol. 2006;7(1):57-66.

664 76. Zhu JW, Brdicka T, Katsumoto TR, Lin J, Weiss A. Structurally distinct phosphatases CD45 and
665 CD148 both regulate B cell and macrophage immunoreceptor signaling. Immunity. 2008;28(2):183-96.

666 77. Takeshita S, Kaji K, Kudo A. Identification and characterization of the new osteoclast progenitor
667 with macrophage phenotypes being able to differentiate into mature osteoclasts. Journal of bone and
668 mineral research : the official journal of the American Society for Bone and Mineral Research.
669 2000;15(8):1477-88.

670 Acknowledgements

671 We thank Arthur Weiss, Kevan Shokat, Yoji Shimizu, Brandon Burbach, Erik Peterson, Juan Rivera,
672 and Ryo Suzuki for reagents and discussion and Terri Kadlecek, Marianne Mollenauer, and Whitney
673 Swanson for technical support. Many thanks also to Hai-Bin Ruan, John Connett, Marc Jenkins, Bryce
674 Binstadt, Erik Peterson, Nicholas Levinson, Aditi Bapat, Frances Sjaastad, and Emily Ewan for valuable
675 discussions and feedback.

676 Funding

677 This work was supported by NIH grants R01AR073966 (TSF), R03AI130978 (TSF) and R01CA215052
678 (KLS) and the following University of Minnesota awards (all TSF): Masonic Cancer Center/American
679 Cancer Society IRG-58-001-55; Grant-in-Aid of Research, Artistry, and Scholarship #92286; University
680 of Minnesota Foundation Research and Equipment Award NF-0315-02; and Center for Autoimmune
681 Diseases Research Pilot Grant 2017. Training support was provided by NIH award T32DA007097
682 (BFB).

683 Author Contributions

684 Conceptualization, Methodology, and Data Curation: BFB, TSF

685 Investigation, Validation, and Visualization: BFB, MGN, TSF

686 Formal Analysis, Writing- Review and Editing: BFB, MGN, KLS, TSF

687 Writing- Original Draft: BFB, TSF

688 Funding Acquisition: BFB, KLS, TSF

689 Project Administration, Resources, Validation, and Software: TSF

690 Supervision: KLS, TSF

691 Competing Interests

692 The authors state that they have no competing interests.

693 Data and Materials Availability

694 Reagents and protocols will be provided upon request.

695 Figure Supplements

696 **Figure 1–figure supplement 1. Loss of positive signaling in c-Cbl-deficient cells prevents**
697 **assessment of LynA contributions to Erk phosphorylation.**

698 **Figure 3–figure supplement 1. LynA^{Y32A} and LynB are expressed more highly in Jurkat cells than**
699 **wild-type LynA.**

700 Source Data

701 Figure 1–Source Data 1

702 Figure 3–Source Data 1

703 Figure 3–figure supplement 1-Source Data 1

704 Figure 4–Source Data 1

705 Figure 5–Source Data 1

706 Figure 6–Source Data 1

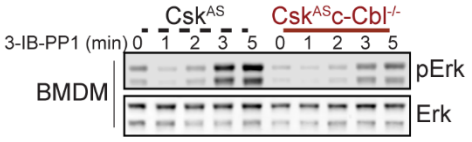

Figure 1–figure supplement 1. Loss of positive signaling in c-Cbl-deficient cells prevents assessment of LynA contributions to Erk phosphorylation. Immunoblot showing impaired Erk phosphorylation in Csk^{AS}c-Cbl$^{-/-}$ BMDMs treated with 3-IB-PP1.

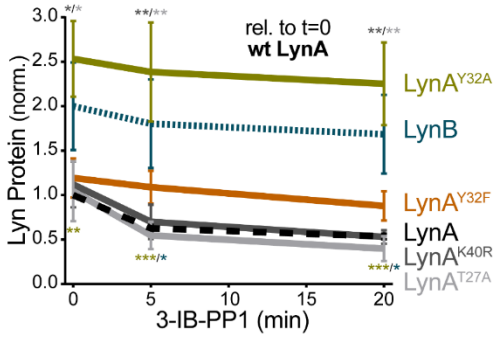

Figure 3–figure supplement 1. LynA^{Y32A} and LynB are expressed more highly in Jurkat cells than wild-type LynA. Quantification of Jurkat-cell LynA protein levels relative to the steady-state overexpression of wild-type LynA protein. Error bars: SEM, N values and data from Fig. 2E-F. Sig. from two-way ANOVA with Tukey's multiple comparison test: [LynA^{Y32A} vs. LynA, olive asterisks], [LynB vs. LynA, teal asterisks], [LynA^{K40R} vs. LynA^{Y32A}, dark gray asterisks], [LynA^{T27S} vs. LynA^{Y32A}, light gray asterisks]; *** P=0.0002-0.0004, ** P=0.0018-0.0062, * P=0.0216-0.0361. [LynA^{T27S}, LynA^{K40R}, and LynA^{Y32F} vs. each other and LynA] and [LynA^{Y32A} vs. each LynB] ns. Refer to Figure 3–figure supplement 1–Source Data 1.